Induced Crystallization and Orientation of Poly(ethylene terephthalate) during Uniaxial and Biaxial Elongation

Yann Marco - Luc Chevalier - Gilles Régnier - Arnaud Poitou*

LMT –Cachan
ENS Cachan/CNRS-UMR 8535/Université Paris 6
61 avenue du Président Wilson
94235 Cachan Cedex (France)
* LTVP
ENSAM Paris
151 boulevard de l'Hôpital
75014 Paris (France)

Summary: Stretching PET at a high strain rate above the glass transition temperature has a positive effect on the strength of the material. In a recent paper[1], we presented the influence of stretch and blow molding parameters on the properties of the final product, especially on the crystallinity induced by stretching. In this paper, we focus on the effects of loading, temperature, elongation and strain rate on macromolecular orientation and crystallization kinetics. We present experimental results from uniaxial and biaxial elongation tests carried out on injected PET specimens. To minimize the effect of quiescent crystallization, specimens are quickly heated with infrared lamps before the test and temperature is regulated during the test.
Both uniaxial and biaxial tests are analyzed using a cross correlation technique[2] that compares a picture used as reference and the picture of the deformed specimen. This technique allows us to determine all strain components at each point of the specimen, even when the strain field is not homogeneous. In a second part, we present measurements of macromolecular orientation and crystallinity ratio performed after each test. The infrared dichroïsm technique is used to determine the orientation of the microscopic morphology of PET before and after the testing. DSC measurements and density measurements are carried out to calculate the crystallinity ratio. Influences of strain rate, temperature and strain path sequence are evaluated in order to build a database for recent models of induced crystallization[3],[4],[5].

Introduction

What we present here is part of a global study of the injection blow-molding process of PET (PolyEthylene Terephthalate) bottles. PET is widely implanted in the plastic bottles market: the consumption of PET bottles increased from 2,8 million tons in 1995 to 5,3 million tons in the year 2000. The optimization of blowing process needs a good knowledge of the different stages of the process and in particular, the associated morphology evolution during stretching and

 CCC 1022-1360/00/$ 17.50+.50/0

blowing.

Blow molding machines make PET bottles from injected preforms. These preforms are heated up and blown up through bi-orientational -longitudinal then radial- stretching. Like most polymers PET has a low heating conductivity. Heating techniques using convection or conduction not only require a long heating time, but also lead to microstructure heterogeneity between the skin and the core of material. An alternative is radiation heating with infrared waves: solution used industrially. It leaves one face of the specimen available for image acquisition with a CCD camera.

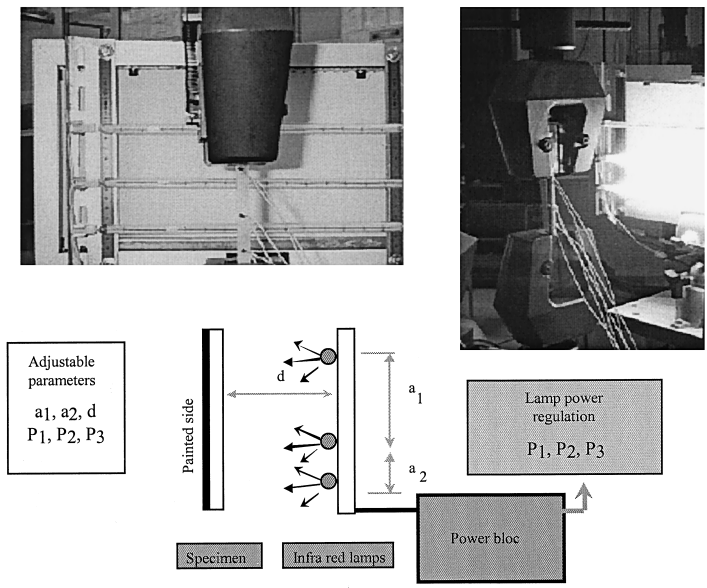

Figure 1: Infra red heating apparatus

The heating apparatus is composed of three lamps. Each one is fed independently and the distances between them are adjusted in such a way as to heat our sample uniformly (Fig. 1). Since we want to have a deep penetration and a maximum absorption whatever the heating power required, we allow an adjustment range of between 65 and 100 % of the maximum voltage. The maximum variation during the test is of ±1° compared to the imposed temperature. The

deformation of the specimen during the test is captured by a CCD camera. To determine the displacement field of one image with respect to a reference image, we consider the image of a square region which from now on will be called the 'zone of interest' (ZOI). The aim of the correlation method is to match the zone of interest in both images. The displacement of one ZOI with respect to the other is reflected by the two-dimensional shift of the intensity signal which has been digitized by the CCD camera. To estimate a shift between two signals, a standard approach is to utilize a correlation function. The theoretical aspects of correlation are developed in a previous paper from Chevalier et al.[2]. The procedure is implemented in Matlab™. The typical results obtained after an uniaxial test is presented in Fig. 2. The precision of the method is at least on the order of 2/100 pixel and the minimum detectable displacement is also in the order of 2/100 pixel.

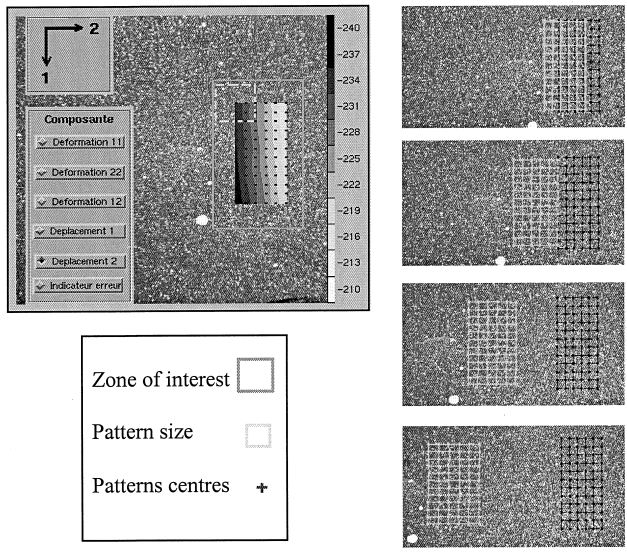

Figure 2: Digital image intercorrelation technique used to measure displacement field (typical uniaxial result)

Uniaxial and biaxial tension tests on PET samples

In this section we present the tension tests carried out to analyze the effects of temperature, elongation speed and loading type (uniaxial, equibiaxial or sequenced biaxial elongations) on

mechanical and microstructural characteristics. Uniaxial tension tests have been carried out at different temperature (from 80 to 110°C) for a wide range of tension speeds (from 0.01 to 1 s^{-1}). Each specimen is stretched from 50 up to 150 mm ($\lambda = 3$, where λ is the elongation) and then strain is maintained while stress relaxes. Typical results are presented in this section.

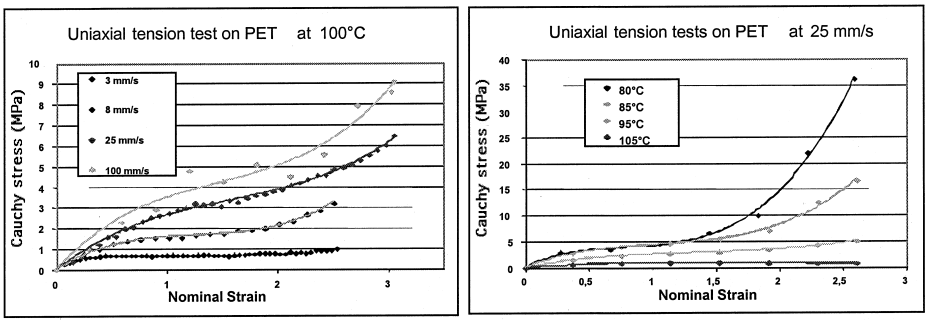

Figure 3: Typical strain-stress curves for PET behavior during tension tests at constant elongation speed

Testing specimen material is a PET given by Eastmann (ref.9921W) which is commonly used for stretch-blow molding. The polymer was dried 12 hours at 160°C. The temperature of the mold was set at 10°C. As the preforms nearly have the same thickness (4 mm) as our injected specimen, we suppose that they share an identical microstructure. More information on the initial microstructure of the specimen will be given in the following sessions. Uniaxial tension tests have been carried out on a MTS 801 hydraulic machine. The load cell used has a 10 kN capacity for all tests. During the first part of the test, we controlled the global displacement to keep the strain rate more or less constant. The second stage is the relaxation step in which the strain remains constant. The strain field is continuously acquired by the CCD camera. We present typical tension and relaxation results and particularly the strain hardening index (SHI) and relaxation characteristics (θ, σ_r) with respect to the strain rate and the temperature imposed during the tension test. In Fig. 3 Cauchy stress is plotted versus elongation λ (i.e. $\lambda=1+\varepsilon_n$), which shows the typical behavior where strain hardening occurs. For all tests performed above the glass transition temperature, tensile load decreases while the temperature increases. It has been admitted that strain hardening effect was due to induced crystallization but some authors[6],[7]

point out in recent papers that macromolecular orientation should explain this strain hardening effect and that crystallization only appears during the second step of the test. As the temperature of the test increases, this strain hardening effect decreases. For example, it does not occur during the test at 105°C. To quantify this effect we define SHI index:

$$SHI = \frac{\sigma(\varepsilon = 2.5)}{\sigma(\varepsilon = 0.25)} \quad (1)$$

In Fig. 4 this index is plotted versus the strain rate for various test temperature. It can be observed that an important jump appears at the glass transition temperature. Indexes for 80°C and 85°C are higher then all others. Above 90°C the increase in temperature is associated with a decreasing index value. Moreover the strain rate has a small influence on index value.

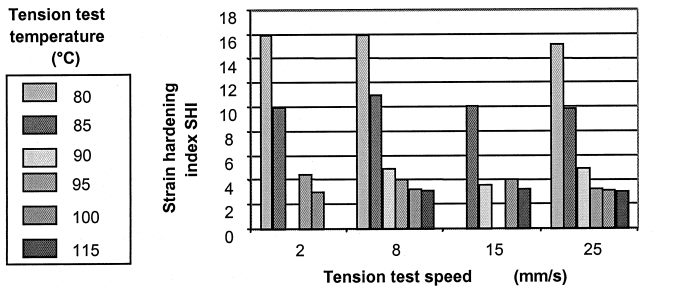

Figure 4: Strain hardening index for given tension test temperature and speed conditions

During the relaxation part of the test, we identified the relaxation time θ and the asymptotic stress σ_r by minimizing the distance between experimental curves and the analytical expression given by the following simple viscoelastic model:

$$\sigma(t) = \sigma_0 - (\sigma_0 - \sigma_r)\left(1 - \exp\left(-\frac{t}{\theta}\right)\right) \quad (2)$$

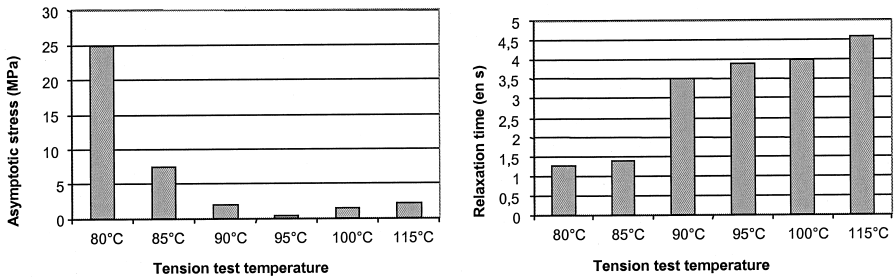

Figure 5: Asymptotic stress σ_r and relaxation time θ for different tension test temperatures at a given speed

The calculation was done for each couple of speed and temperature. Figure 5 shows the relaxation time values versus the strain rate at various temperatures. It clearly shows that near the glass transition threshold, relaxation times are low and the influence of the strain rate is minimal. At higher temperatures, the relaxation time increases and the influence of speed is greater. For a given temperature, the relaxation time decreases with the strain rate.

The biaxial tests presented here have been carried out on a triaxial testing machine Astree (Fig. 6). This electro-hydraulic testing machine has six servohydraulic actuators. This machine has been developed by LMT-Cachan and Schenck AG, Darmstadt, Germany. A hydraulic power station generates a maximum flow of 330 l/mn. Closed loop control for each actuator is provided by a digital controller. The controller monitors and provides signal conditioning for each load actuator position channel. Each axis (X_1, X_2 and X_3) has its own dedicated strain channel for signal conditioning and control. Strain input signals can be generated through a variety of strain measuring devices such as strain gages, extensometers, etc. Computer test control and data acquisition are performed by an object-oriented programming software, LabVIEW®.

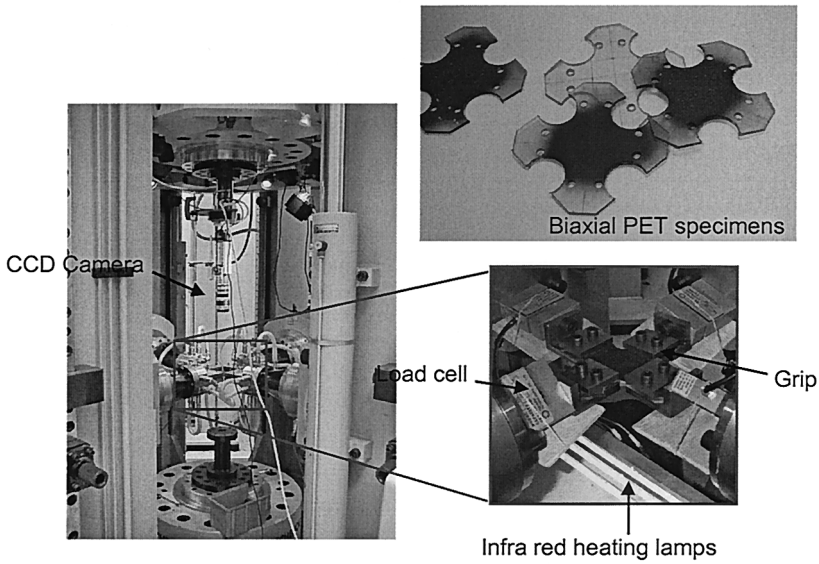

Figure 6: Biaxial testing aparatus, triaxial testing machine Astree, biaxial specimens, IR heating apparatus

Figure 6 shows the disposition of the PET specimen in the grips, the load cells, the CCD camera and the infrared heating system. Since the grips are not translucent to infrared light, we only heat and deform the test zone of the specimen. Therefore we can avoid the shrinkage and the slipping in the grips. Two designs of biaxial tension-test specimen were used (see Fig 6) in order to get maximum elongation.

Two kinds of biaxial tension tests were carried out at different temperatures (90 and 100°C) and elongation speeds (8, 20 and 40 mm/s). In a first equi-biaxial test, the specimen was simultaneously stretched in both perpendicular directions X_1 and X_2. In a second test, we stretched the specimen in X_2 direction first and then in X_1 direction in order to reach the same state of deformation. Figures 7 and 8 present the two biaxial tests.

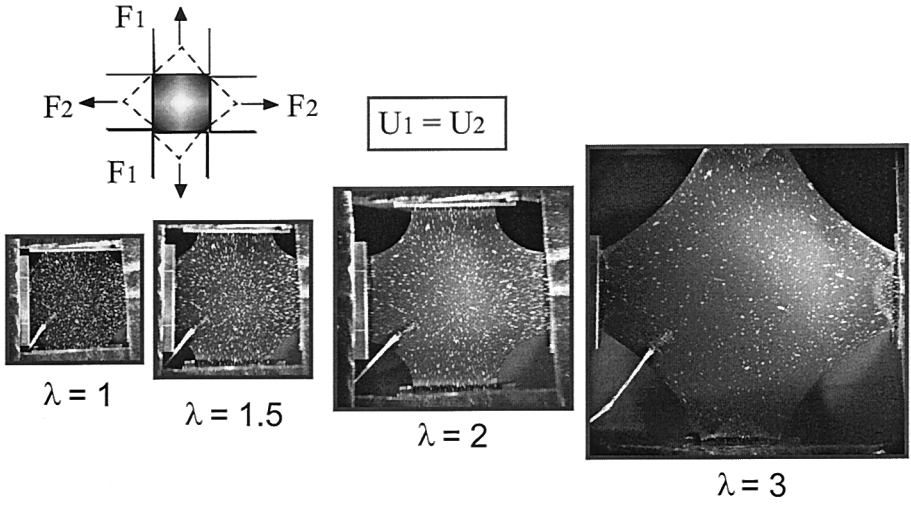

Figure 7: Typical equibiaxial elongation test

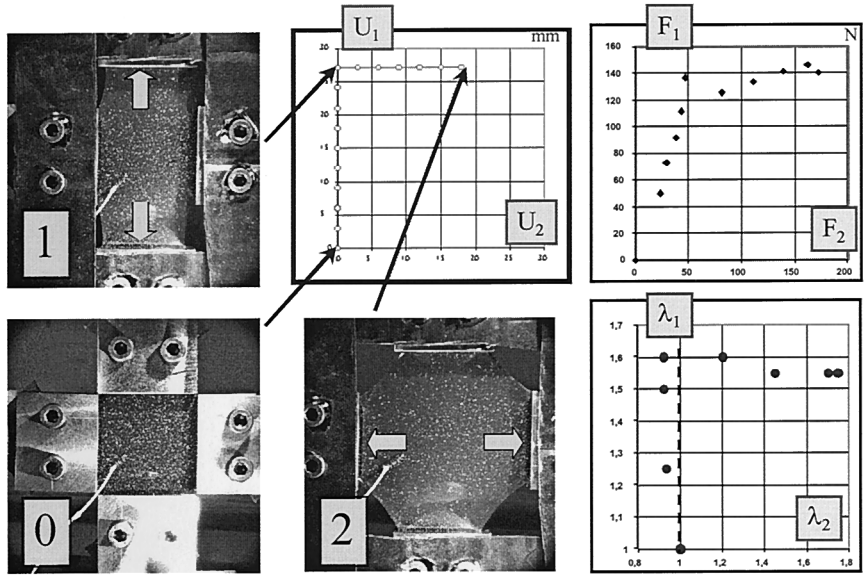

Figure 8: Sequential biaxial loading, Grip displacement U_1 and U_2, Load F_1 and F_2, Elongation in the central region of specimen λ_1 and λ_2

As in the uniaxial tension test, both tests show a strain hardening effect and the combined influence of temperature and strain rate. Figure 9 presents the results of the equi-biaxial test. One can observe that the influence of speed and temperature is the same as in the uniaxial tension tests. In superposition the first step of sequential biaxial tension is plotted. It is worth noting that the elongation in the central region is lower than the final elongation in the same direction during biaxial testing. This is obviously due to poor boundary conditions in the fixed grips. We can also observe that for the same elongation, the stress is lower. This is a classical result for plane strain in regard of equibiaxial strain even if some shearing appears from boundary conditions.

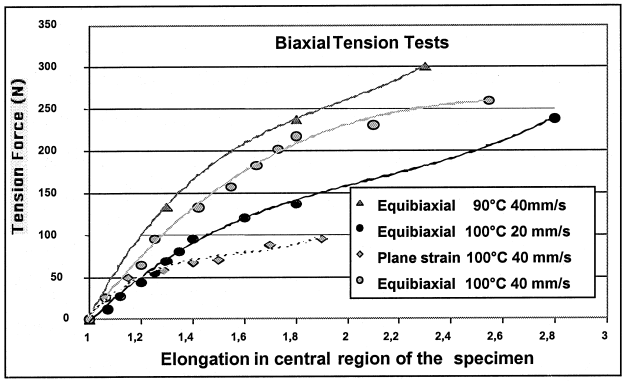

Figure 9: Strain-stress curves obtained from equibiaxial and plane strain (i.e., first step of biaxial sequential test) tension tests

Figure 10 shows typical results obtained by Correli, our digital image correlation software. The displacement fields are clearly non-homogeneous in both biaxial tests, and should lead to data treatment through a comparison with numerical simulations, as it has been done previously on natural rubber[8]. It is possible to evaluate the strain-stress behavior of the PET in simultaneous equibiaxial tests. Assuming stress is almost constant on the first diagonal of the specimen (which is confirmed by the strain homogeneity revealed by image correlation), the biaxial σ_{BT} Cauchy stress from tension load F is given in the following relation:

$$\sigma_{BT} = \frac{\sqrt{2}F}{eL} \tag{3}$$

L is the diagonal length and e the thickness of the specimen. With the incompressibility

hypothesis, we can determine e from elongation λ. On strain-stress curves (Fig. 11) we can compare biaxial and uniaxial behaviors. This confirms that for identical conditions (same elongation, speed and temperature), uniaxial response is almost twice as weak as the biaxial one.

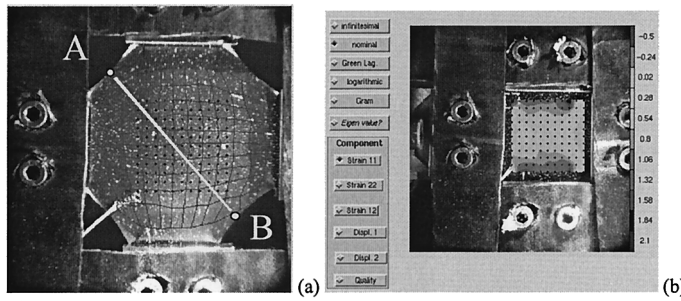

(a) (b)

Figure 10: Typical inter-correlation result for the equibiaxial test
(a) Typical displaced grid for equibiaxial testing, Assuming stress is also constant along AB, one can obtained Cauchy stress from force F
(b) ε_{11} nominal strain component, one can see that this component is quite constant along AB.

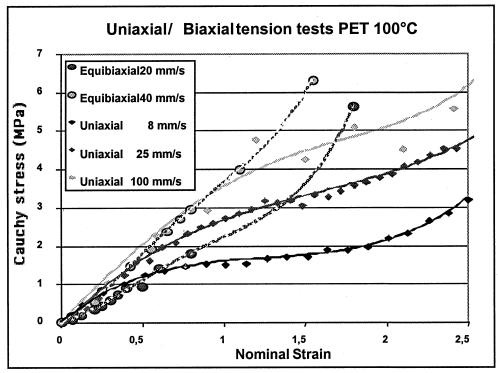

Figure 11: Comparison of elongation speed effect on Uniaxial/Biaxial behavior of PET at 100°C

Morphology modification during PET testing

In this section we present the morphology of injected PET before our elongation tests. Density measurements carried out on thermally crystallized samples allow us to identify an Avrami model

for crystallization kinetics. We used infrared dichroism experiments to identify the initial orientation of these specimens. In a second part, induced orientation and crystallization are examined versus elongation conditions.

PET samples, cut out from injected specimen and almost completely amorphous (less than 3 % crystallinity) are heated in a thermal oven. The oven enables us to control the temperature to within about a half-degree. Samples are then taken out from the oven at specific times. They are immediately immersed into cold water to stop the morphology changes. Crystallinity is measured by differential densimetry. Five different heating temperatures (90, 100, 105, 110 and 115°C) were tested. The curves in Fig. 12 show the crystallinity ratio evolution versus time. Induction times, which one classically finds for the curves of thermal crystallization, are very small here. This is certainly due to the low but nonzero initial crystallinity ratio in our injected specimen.

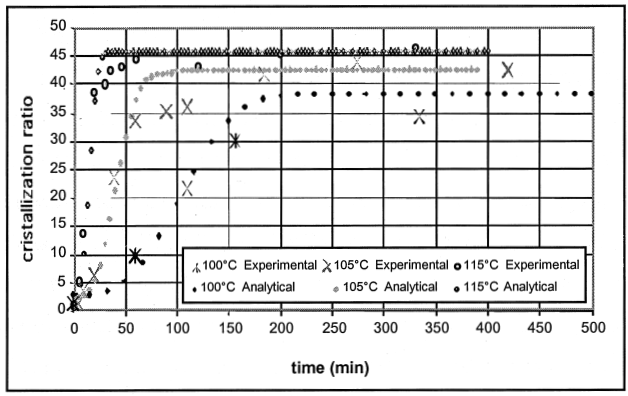

Figure 12: Experimental and analytical crystallization kinetics for some temperatures

The identification of k and n parameters in Avrami's model shows that with the usual value of n=3 model does not exactly fit on the whole curve (Fig. 12). In particular, we can see that experimental data present a lack of crystallization kinetics when the ultimate crystallization is nearly obtained. This effect is traditionally explained by secondary interlamelar crystallization (see for example [9],[10],[11]).

Table 1: k values for our PET transformed in λ_k and compared with Hieber's values[12]

Temperature (°C)	k	λ_k (min)	λ (min)
100°C	0,0000006	119	125
105°C	0,00001	46	40
110°C	0,00007	24	25
115°C	0,0002	17	10

In addition Table 1 shows the important influence of temperature on parameter k: the higher the heating temperature, the faster crystallization spreads. Hieber[12] collected important experimental results and plotted them as parameter λ versus temperature. Parameter $\lambda(T)$ is related to k and n by the following relation:

$$\lambda = \frac{1}{k^{1/n}} \tag{4}$$

Identified values of k leads to λ values coherent with those collected by Hieber. The experimental study also gives us ultimate crystallinity ratios.

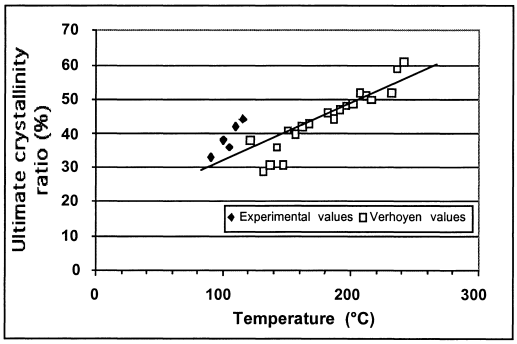

Figure 13: Ultimate crystallinity ratio dependence on temperature

Figure 13 compares the DSC measurements of the ultimate crystallinity for various temperatures with Verhoyen's results[13]. Our experiments do not match exactly Verhoyen's data. However, they remain in the range of variation of his measurements from one temperature to another and can thus give some tendencies for temperatures close to the glass transition Tg.

As a partial conclusion, this study of thermal crystallization of PET allows us to validate the experimental protocol we used by comparing our values with those in the bibliography. It clearly

appears that thermal regulation using convection heating is too long to assure that no quiescent crystallization superpose flow induced crystallization during elongation tests. Our choice, infrared heating, appears to be quick enough to solve this problem. In addition, the comparison of the experimental curves with simple models of the Avrami type or Nakamura, confirms the failure of these models to take the secondary crystallization into account. Lastly, the study of the ultimate crystallinity makes it possible to prolong Verhoyen study for temperature near the glass transition. Infrared spectroscopy is based on a selective absorption of monochromatic radiation by a portion of molecule. Jasse and Koenig[14] indicate that 1340 cm^{-1} corresponds to 'trans' conformation of CH_2 group, which can easily crystallize. 875 cm^{-1} and 1020 cm^{-1} peaks are associated with benzene ring as well as 1420 cm^{-1}. For that last peak, Cole et al[15] precise that its intensity is neither sensible to crystallization, nor orientation. Infrared dichroism measurements are carried out to evaluate specimen's orientation given via the harmonic functions P_2:

$$f = \frac{3 < \cos^2\theta > -1}{2} = P_2(< \cos^2\theta >) \qquad (5)$$

The chosen thickness for our PET samples is 10µm. Results have been obtained for an almost amorphous specimen, a slightly crystallized specimen (100°C for 90 min), a strongly crystallized specimen (130°C for 3 hours). If we focus on the dependence of intensity of 875, 975, 1020 and 1340 cm^{-1} peaks with respect to crystallinity (Fig. 14), it appears that 1340 peak is very sensitive to thermal crystallization. One can suppose the others will represent amorphous phase or average value between crystallized phase and amorphous phase orientation.

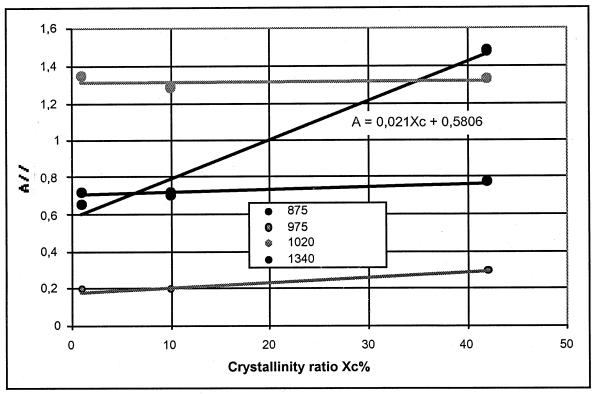

Figure 14: Influence of thermal crystallization: influence on peak absorbance

As a partial conclusion of this part, we show (Fig.15) this orientation function for 4 given peaks versus depth from the injected specimen skin. It can be seen that neither for the injected specimen nor for the thermally crystallized one, orientation can be observed.

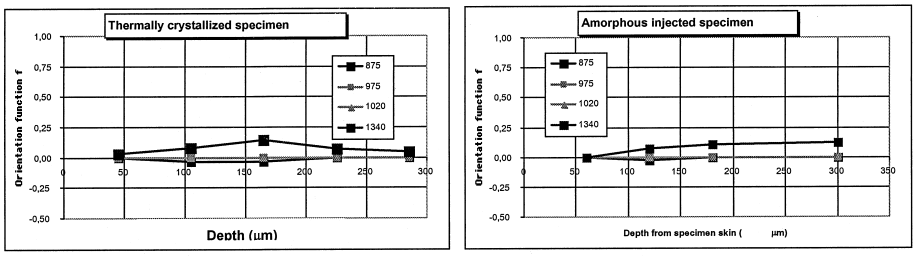

Figure 15: Macromolecular orientation in thermally crystallized PET specimen (left) and non stretched amorphous specimen (right)

Density and infrared dichroism measurements have been done on the uniaxialy and biaxialy stretched specimens in order to quantify the effect of tension conditions on induced crystallization and morphology changes. The typical result obtained from uniaxial tests (Fig. 16) is that strain rate as an increasing effect on crystallization kinetic as temperature as the opposite effect from Tg to higher values. These results are to be compared with the one related to relaxation time: as tension test temperature growths, relaxation time decreases which is representative of a macromolecular mobility. This mobility is reduced if crystallization occurs during elongation and changes the material morphology. For high temperature (20°C above Tg), relaxation is easier and elongation of the specimen is not enough to change the material morphology. Very small induced crystallinity is observed and typical relaxation time is equal to amorphous phase relaxation time.

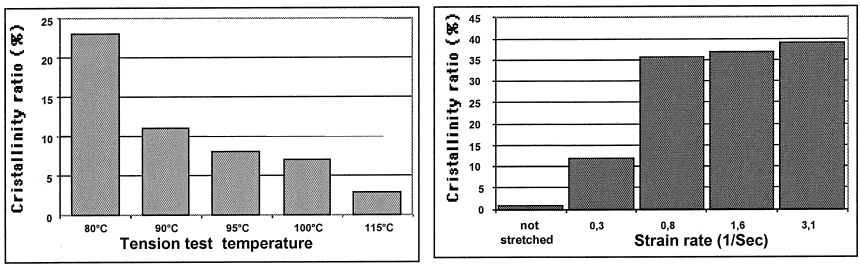

Figure 16: (left) Influence of thermal conditions on induced crystallization for a given tension test elongation speed (8 mm/s) (right) Influence of strain rate conditions on induced crystallization for a given test temperature (90°C)

Figure 17 shows crystallinity measurements done on samples cut off the central zone of biaxial elongation tests. Since thickness is different from uniaxial tension test specimen, we also made density measurements on non deformed specimens to confirm the low initial level of crystallinity before elongation. The first chart (top left) shows the increasing effect of strain during an equibiaxial test on induced crystallinity for identical values of strain rate, temperature. The elongation ratio corresponding to high strain is about 3 since the one corresponding to low strain is about 2. As in uniaxial elongation, if we admit that crystallinity ratio is correlated with strain hardening, it appears that during the first stage of elongation no consequent morphology change can be detected. Strain hardening and crystallinity increasing appears during the second stage of elongation: typically above $\lambda = 2$. For high strain, top-right chart in Fig.17 shows the influence of strain rate. As speed increases, final crystallinity is higher. Of course this correlation saturates for very high tension speed since ultimate crystallinity ratio is an upper bound. In low-left chart, the effect of temperature is illustrated on two sequential biaxial tests. This result has also been observed on equibiaxial tests: as temperature increases, induced crystallinity decreases. The last (low-right) chart gives a comparison between equibiaxial and sequential biaxial tests. This final observation has to be confirmed, it is in fact very difficult to manage the same final strain field for both kinds of test. It seems that initial orientation during the first stage of the sequential biaxial test helps induced crystallization during the second stage. The sequence leads to an higher final crystallinity ratio.

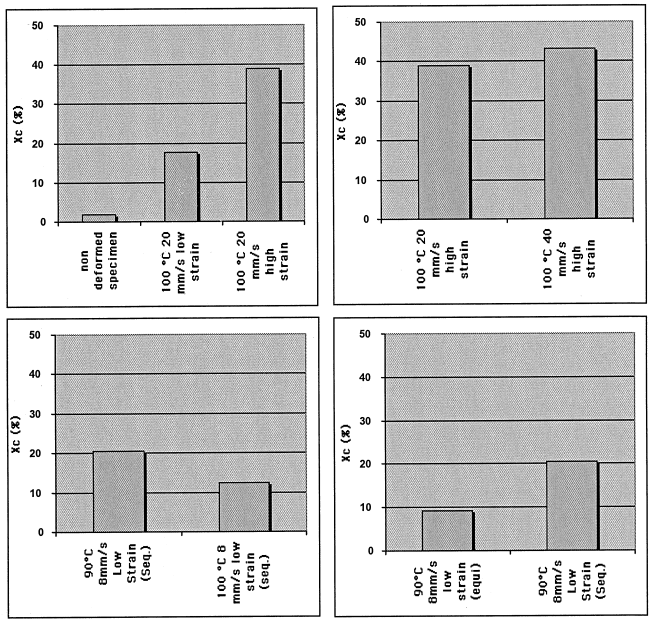

Figure 17: Influence of elongation, strain-rate, temperature and strain sequence on induced crystallization.

10 μm thick samples have been cut out the uniaxially stretched specimens. As different strain rates and temperature have been used for these elongation tests, final orientation is different from a specimen to another. Figure 18 charts show the influence of the sample position in the specimen depth. One can notice that orientation is not very dependent of sample position which is quite different from what can be observed for injected samples[16]. This confirms a posteriori the temperature homogeneity obtained by the infrared heating apparatus. Orientation can thus be represented by only one variable f for the all specimen description, since then one can study the influence of strain rate and temperature on this variable. Let us notice that orientation values obtained with 875 and 1020 peaks are quite similar, that confirms those two peaks represent the same chain element vibration. For specimens stretched at 105°C quasi no orientation is observed but those stretched at 90°C have an obvious orientation in the elongation direction for the same strain rate. The influence of temperature on orientation appears to follow the same rules than for crystallization ratio: the effect is more important for temperature near Tg and quickly decreases when temperature rises up to 100° or more. For the same temperature (90°C) the influence of

strain rate is also similar to crystallinity ratio evolution: as elongation speed increases, as orientation is important.

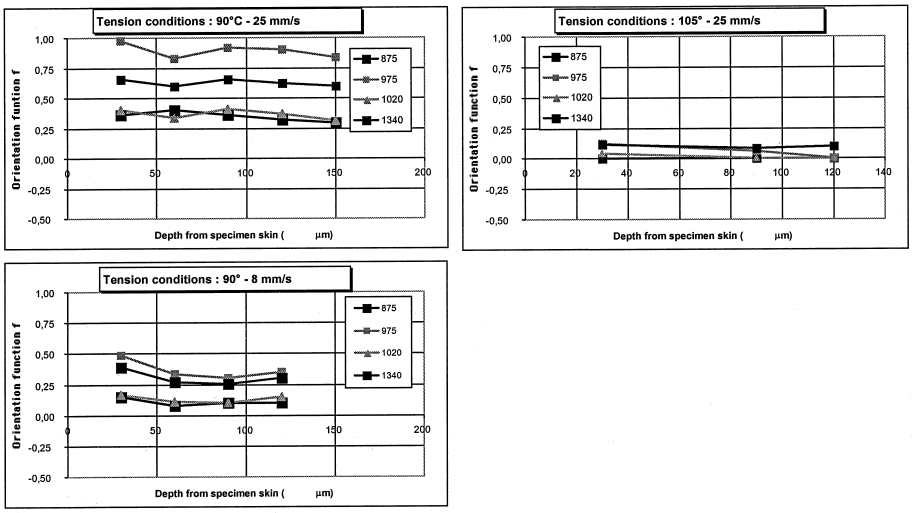

Figure 18: Influence of uniaxial testing conditions on macromolecular orientation. On top plots one can see that from 90° to 105° the final orientation decreases nearly to 0. On left plots one can see a similar influence due to decreasing of tension speed.

Once again, the conjugate effect of temperature and speed is highlighted: orientation appears for high strain rate and for low temperature (till it remains over Tg). Orientation values obtained with 1340 and 975 peaks are higher than the one calculated with 1020 or 875 cm^{-1} peaks. This can be explained with the partial induced crystallization of the specimen since 1340 cm^{-1} peak is very sensible to crystallinity ratio. For a given crystallization ratio Xc, the average orientation is obtained by relation:

$$f = X_c f_c + (1 - X_c) f_a \qquad (6)$$

From Eq. 6 it is easy to extract the orientation f_c of the crystalline phase. Let's examine the 90°C specimen stretched at 25 mm/s: the density measured showed an induced crystallization ratio up to 35%. According to Cole and al., if we make the assumption that 1020 and 875 cm^{-1} peaks represent the amorphous phase orientation (f_a = 0.4) and that 1340 cm^{-1} is representative of the

average orientation (f = 0.6), it appear that the crystalline phase is nearly completely oriented in the stretching direction (f_c = 0,97). This result is confirmed by the orientation value given by the 975 peak which is very high also and in the same range than f_c. The natural conclusion is that this peak should be representative of the crystalline phase.

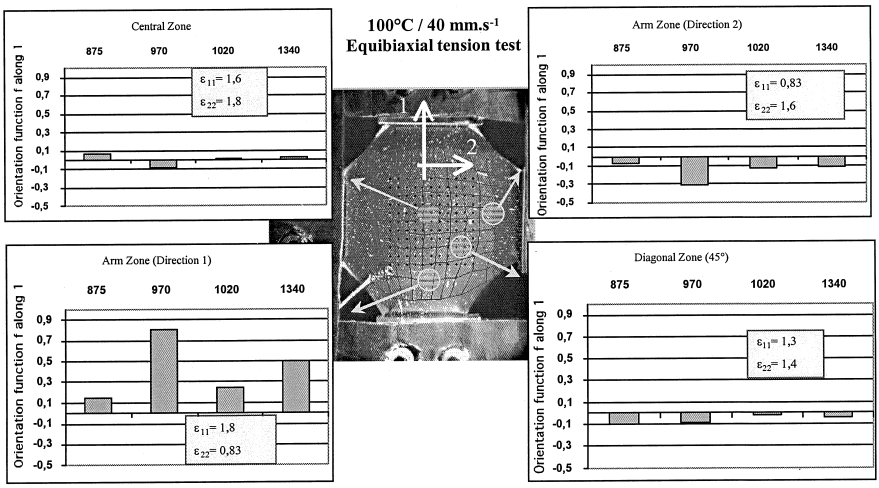

Figure 19: Orientation function for different positions in the non homogeneous strain field

Figure 19 shows orientation function values issued from measurements made on samples cut in biaxialy stretched specimens. On the central picture, one can see the location of samples. It is worth noting that in the central region (upper left chart) as well as for the diagonal zone (lower right chart) no significant orientation can be highlighted. Macromolecules are stretched but orientation function is not representative of this macromolecular elongation. Since the global study final goal is to make correlation between induced mechanical properties with respect to stretching conditions, orientation function is not the good variable. Direction 1 is the parallel direction, direction 2 is the orthogonal one. Orientation values obtained from the 970 cm^{-1} peak shows that the crystalline phase is oriented (f = 0.8) in the elongation direction 1 in the arm zone of the lower left chart. As well the arm zone of the upper right chart shows that crystalline phase is oriented in the elongation direction 2 (f = -0.3). Since the biaxial test does not lead to an homogeneous strain field, the orientation is very similar to the one measured after uniaxial tests.

Both arms are uniaxialy stretched. One can see that the 970 cm^{-1} peak is the most sensitive to the small difference of nominal strain in 1 and 2 directions. This comparison remains qualitative because strain rate and temperature conditions are not identical from a test to another. Nevertheless, when strain is higher in direction 1 it appears that the orientation function is positive. Orientation values become negative when strain in direction 2 becomes higher than strain in direction 1. For identical strain rate, testing temperature also influences the effect of a difference between direction 1 and 2 elongations on orientation function. For temperature near Tg (90°C) a small elongation difference leads to an important value of orientation function. The same elongation difference has a smaller effect when testing temperature is higher (100°C for example). This is one more strain rate - temperature opposite influence.

Conclusions

Blow molding process generates major mechanical properties modifications linked to thermo mechanical history of the material illustrated by induced crystallization and macromolecular orientation. A complete range of uniaxial elongation tests has been carried out and correlation between strain induced crystallization and orientation with the mechanical behavior of PET during the test has been presented.

The effects of tension speed and temperature during the test on final morphology have been highlighted. Biaxial elongation tests have been achieved using infrared heating apparatus and image correlation technique for strain field calculation during the test. Different complex path of biaxial can be managed: equibiaxial and sequential biaxial elongation tests have been presented. Morphology measurements on biaxialy stretched samples have been presented in terms of crystallinity measured by density and orientation function measured by infrared dichroism.

First results have been discussed in regard with mechanical properties. Further work in this field will be done to improve strain induced crystallinity modeling.

Acknowledgement

To Eastmann who provides PET for injection.

To Pierre and Laura for English corrections.

[1] L. Chevalier, *Plastic, rubber and composite Processing and application* **1999**, *28*, 385.
[2] L. Chevalier, S. Calloch, F. Hild, Y. Marco, *Eur. J. Mech. A/solids* **2001**, *20*, 169.
[3] A.K. Doufas, I. S. Dairanieh, A. J. McHugh, *J. Rheol.,* **1999**, *43*, 85.
[4] A. Poitou, A. Ammar, *C.R.Acad.Sci.* Paris, **2001**, t329 série IIb, 5.
[5] G. Eder, H. Janeschitz-Kriegl, *Material science and technology* (ed. H. Meijer), Verlag Chemie, Weinheim, **1997**, *18*, 269.
[6] A. Mahendrasingam, C. Martin, W. Fuller, D.J. Blundell, D. H. MacKerron, J. Oldman, J. L. Harvie, D.H. MacKerron, R. C. Riekel, P. Engström, *Polymer* , **1999**, *40*, 5553.
[7] J.A. Pople, G.R. Mitchell, S.J. Sutton, A.S. Vaughan, C.K. Chai, *Polymer*, **1999**, *40*, 2769.
[8] L. Chevalier, Y. Marco, in press on *Polymer Engineering and Science*, April 2001.
[9] F.P. Price, *J. Polym. Sci. Part A - Polym. Chem.*, **1965**, *3*, 3079.
[10] C.N. Velisaris, J.C. Sefaris, *Polym. Eng. Sci.,* **1986**, *26*, 1574.
[11] F. Dupret, L. Vanderschuren, *AIChE J.,* **1988**, *34*, 1959.
[12] C.A. Hieber, *Polymer*, **1995**, *36*, 1455.
[13] O. Verhoyen, Crystallization of PET in Injection Molding: Experiments, Modelling and Numerical Simulation, PhD Thesis, University Catholique de Louvain, Belgium, 1997.
[14] B. Jasse, J.L. Koenig, *J.Macromol.Sci. – Rev.Macromol.Chem.*, **1979**, *C17(1)*, 61.
[15] K.C. Cole, J. Guevremont, A. Ajji, M.M. Dumoulin, *Applied Spectroscopy*, **1994**, *48*, 1513.
[16] G. Regnier, T. Delebecque, L. Chevalier, Molecular orientation of injected non-filed semi-crystalline polymers, EPS 2000 - Guimares (Portugal), Sept. 2000